2021 43rd Annual International Conference of the
IEEE Engineering in Medicine & Biology Society (EMBC)
Oct 31 - Nov 4, 2021. Virtual Conference

Patient-Specific Anisotropic Volume of Tissue Activated with the Lead-DBS Toolbox

Roberto Garza[1,2], Alba Segura Amil[1,2], Andreas Nowacki[1], Claudio Pollo[1], T. A. Khoa Nguyen[1,2*]

Abstract— **Deep brain stimulation is an effective neurosurgical intervention for movement disorders such as Parkinson's disease. Despite its success, the underlying mechanisms are still debated. One tool to better understand them is the Volume of Tissue Activated (VTA), that estimates the region activated by electrical stimulation. Different estimation approaches exist, these typically assume isotropic tissue properties and modelling of *anisotropy* is often lacking.**

The present work was aimed at developing and testing a method for patient-specific VTA estimation that incorporated an anisotropic conduction model. Our method was implemented within the open-source toolbox Lead-DBS and is accessible to the public.

The present method was further tested with two patient cases and compared to a standard Lead-DBS pipeline for VTA estimation. This showed encouraging similarities in one test scenario and expected differences in another test scenario. Further validation with a wider cohort is warranted.

I. Introduction

Deep Brain Stimulation (DBS) is a state-of-the-art neurosurgical intervention. It has shown to be an effective tool in treating a variety of diseases. An extensive review of its success for movement disorders can be found in [1].

To better understand the effects of DBS, the Volume of Tissue Activated (VTA) has been a very helpful model. For instance, in [2] a patient-specific computational model of DBS to estimate VTAs is reported. The model incorporated diffusion-weighted images but required considerable expertise to be implemented [3]. In contrast, the estimation of VTAs has recently become more accessible to a wider research community through the Lead-DBS toolbox requiring markedly less computational expertise and resources [4].

This toolbox mainly estimates the VTA by computing and thresholding the electric field generated by the stimulation. The electric field depends on the conductivity of the tissue. The default estimation in Lead-DBS can account for the conductivity of white and grey matter and is assumed to be isotropic, i.e., identical in all spatial directions. This assumption and the resulting VTAs have served to better understand DBS, when targeting grey matter nuclei such as the subthalamic nucleus for movement disorders [5]. However, some more recent DBS indications have been explicitly targeting white matter tracts such as the dentato-rubro-thalamic tract for essential tremor [6], [7] or the medial forebrain bundle for depression [8]. Such white matter tracts typically exhibit highly anisotropic conductivity [9], i.e., different values in different spatial directions. Therefore, a patient-specific and anisotropic conduction model may improve the VTA estimation and may eventually help improve DBS programming and patient outcome for these indications.

The present work aimed to develop a VTA estimation method (referred to herein as Anisotropic method) with the following features:

- patient-specific and anisotropic conduction model;
- implemented in Lead-DBS to be available to a wider research community.

II. Methods

This work is organized in three steps. First, we describe the preprocessing of the patients' structural and diffusion images as well as the anisotropic conduction model. This is necessary to extract the anisotropic properties of the brain tissue. Second, we introduce the core elements of the Anisotropic method, i.e., we describe the conduction model, the electric field computation and the thresholding for VTA estimation. Finally, we specify two test scenarios that compares the Anisotropic method with a standard Lead-DBS estimate of VTA.

A. Preprocessing

We extracted anisotropic electrical properties from diffusion images. Images from two patients, previously published in other cohorts [5], [6], were used to develop and test the Anisotropic method. Besides standard structural T1 and T2-weighted sequences, diffusion images were recorded. For patient A these were characterized by 62 gradient directions, b-value 1000 s/mm^2, slice thickness 4 mm and slice resolution 1 mm; for patient B 64 gradient directions, b-value 1000 s/mm^2, slice thickness 2 mm and slice resolution 1 mm. After acquisition of the 4D diffusion images, the MRtrix [10] and FSL [11] software was included in the preprocessing pipeline:

1. Denoise and unring using MRtrix [12];
2. Perform eddy correction using topup [13], [14] and eddy [15] with FSL. In case the reverse mode acquisition was not available, topup was substituted by Synb0-DisCo [16] (this was the case for both patients A and B);
3. Extract brain from the structural images and the average null-gradient volume in the diffusion-image with FSL bet [17];
4. Compute the coregistration transform from null-gradient diffusion image to structural image. FSL flirt [18],

[1]Department of Neurosurgery, University Hospital Bern, Switzerland. [2]ARTORG Center for Biomedical Engineering, University of Bern, Bern, Switzerland. *Corresponding author thuyanhkhoa.nguyen@insel.ch.

Research supported by the Swiss National Science Foundation, project number 186142.

[19] with 6 degrees of freedom was used for initialization, and refinement was carried out by a second run of flirt using boundary-based registration algorithm (using white matter segmentation [20]);

5. Apply transform to all the diffusion-image data;

6. Compute voxel-wise diffusion tensor using fanDTasia library for Matlab [21].

The patients' lead reconstruction was obtained using the standard pipeline implemented in Lead-DBS [4].

B. Conduction Model

The conduction model was built upon a tetrahedral mesh designed with the iso2mesh library [22]. From the reconstruction of the leads inside the brain volume, the mesh was computed in native patient space. An initial mesh, which had nodes uniformly distributed over a cylinder with radius 20 mm and height 35 mm centered on the lead, was merged with the nodes of the lead model.

Then each node was assigned its corresponding conductivity tensor. During preprocessing, diffusion-image data was registered to native space. The correspondence between the nodes of the mesh and the relative diffusivity tensor was found using a Nearest Neighbour algorithm. A linear relationship was then used to derive the conductivity tensor from the diffusivity tensor for each voxel. This relationship assumed myelinated axons with an average diameter of 5.7 µm [23]. For the conductivity tensor a geometrical anisotropy model with 6 degrees of freedom and 3x3 positive-definite tensor was adopted [24].

To complete the model, the conductivity tensor was overwritten for nodes that represented the lead and scar tissue.

C. Electric Field Computation and Thresholding for VTA

The model described so far was employed in the computation of the electric field. In fact, with the assumption of large fibres and a specific pulse-width, neural activation can be inferred from thresholding the electric field [25], i.e. the gradient of the electric potential. This threshold depends on the characteristics of the fibres and can be extracted from precomputed tables [26]. The threshold does not depend on the stimulation amplitude.

This approach is also used in a standard Lead-DBS method to estimate VTAs: SimBio/Fieldtrip [27]. Elements having an electric field gradient larger than or equal to 0.2 V/m (the default value, which can be adapted indeed) are assigned to the VTA (Fig. 1). Our anisotropic method used the same threshold for comparison.

D. Testing

Two tests were carried out inspecting: (i) the correct functioning of the overall method (Test 1, 'unit testing'); and (ii) the impact of anisotropy (Test 2).

In both tests, comparisons were run against the SimBio/FieldTrip method in Lead-DBS. In Test 1 the Anisotropic method was fed with a synthetic input that mimicked SimBio/FieldTrip conditions as much as possible (isotropic, tissue-dependent conductivity), though there was a difference in mesh density for the two methods. Specifically, the anisotropic conduction model had a mesh density of around 1.7 nodes/mm^3 in the cylinder, while in the lead it was 2587 nodes/mm^3. The SimBio/Fieldtrip mesh had the same density for the lead, but a value of 287.4 nodes/mm^3 for grey matter regions derived from the DISTAL atlas [28] and 0.3 nodes/mm^3 in the rest of the cylinder. In summary, Test 1 may be regarded as a unit test. In Test 2 in contrast, the patients' diffusion images were integrated (while scar tissue was neglected).

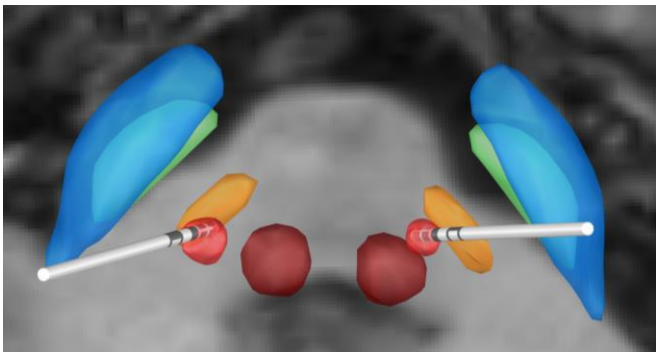

Figure 1. DBS simulation in native space. The model of the leads is represented along with the VTA computed by the Anisotropic method (light red). All the other structures are extracted from the DISTAL minimal atlas. In particular, the blue volume represents the external Globus Pallidus, the green one is the internal Globus Pallidus, the orange one is the subthalamic nucleus and the dark red one is the red nucleus.

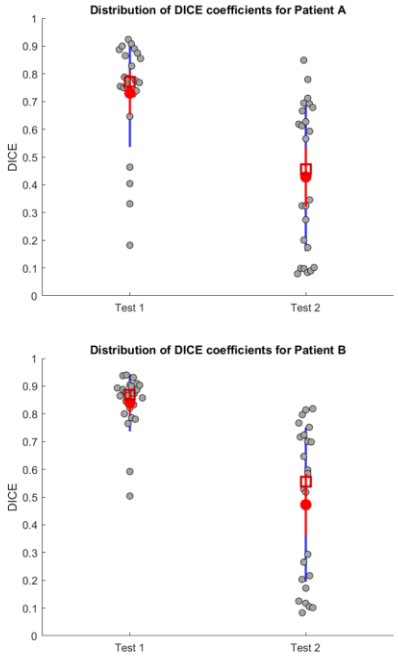

Figure 2. DICE coefficient comparing the VTAs obtained by SimBio/FieldTrip method against the present Anisotropic method in the conditions of Test 1 and Test 2 for the two patients. Mean value is denoted by the red circle, while median is represented by the red square.

In both tests, we performed simulations in voltage-controlled and current-controlled modes at 1, 3, 5 V and 1, 3, 5 mA, respectively. We repeated these conditions for ring and for directional stimulation and in both hemispheres, totaling 2 modes x 3 amplitudes x 2 direction-modes (ring/directional) x 2 hemispheres x 2 patients = 48 simulations for both Test 1 and Test 2. The degree of similarity was assessed by the DICE coefficient.

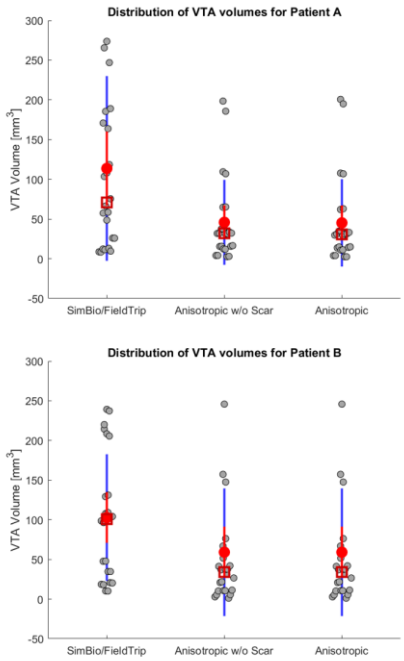

Figure 3. Distribution of the VTA volumes from the three estimation methods used for Patient A (top) and Patient B (bottom). We considered both the Anisotropic method with and without scar tissue modelling. Mean value is denoted by the red circle, while median is represented by the red square.

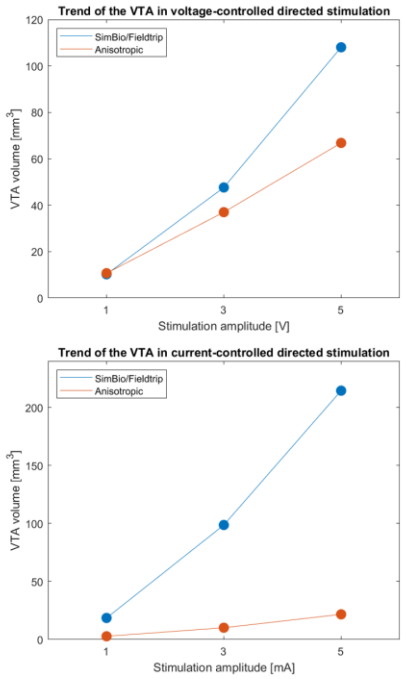

Figure 4. The upper plot shows the growth in volume of the estimated VTAs for different voltages, the lower one for different current amplitudes. The smaller VTA volumes with Anisotropic method were in agreement with a previous report [2].

E. Implementation and Data availability

The present method with further documentation is publicly available on GitHub, implemented within Lead-DBS v2.3.2 (https://github.com/CapriolоSaggio/leaddbs).

The anonymized patient images can be requested from the corresponding author.

A graphical user interface allows adjusting the algorithm's parameters. The present method can be chosen by selecting the Anisotropic option from the Model drop-down menu present in Lead-DBS Stimulation GUI. Typical run times on a PC with 3.4 GHz Intel Core i5 processor and 16 GB RAM were about 360 s on the first run and about 30 s at successive runs, when the computed conduction model was reused.

III. Results

Since this was a preliminary study with a focus on the development of the anisotropic method, we report the results on the two tests.

Fig. 2 shows that the unit test Test 1 yielded median DICE coefficients of 0.79 and 0.87 for patients A and B, respectively.

Test 2 integrated the patients' diffusion images and resulted in DICE coefficients of 0.42 and 0.56 for patient A and B, respectively.

We chose not to report statistical tests, as there is no commonly-accepted similarity threshold for DICE coefficients. Therefore we had reservations about testing these values against arbitrarily set thresholds.

In terms of volume, Fig. 3 shows a reduction in median VTA volume obtained with the Anisotropic method (with and without scar tissue) compared to the outcome of SimBio/FieldTrip.

IV. Discussion

The described anisotropic method underwent preliminary testing. Systematic studies are warranted using a larger cohort to robustly compare the Anisotropic method against alternative algorithms. Furthermore, a thorough analysis regarding the impact of image quality on the outcome of the method would be beneficial.

Test 1 yielded median DICE coefficients of 0.79 and 0.87 for patients A and B, respectively. This test was designed as a unit test of the anisotropic method and high similarity was expected (Fig. 2). These values are encouraging, while the use of different algorithms and conduction models are likely to account for the difference of about 0.2 (a DICE coefficient of 1 means perfect match).

Test 2 yielded a lower median DICE coefficients of 0.42 and 0.56 for patients A and B, respectively (Fig. 2). This represented a marked difference in VTAs due to anisotropy. We noticed a bimodal distribution of DICE coefficients, that was likely associated with stimulation modality. However, our test data set of two patients was too small to draw robust conclusions and further research is necessary.

A qualitative assessment of the estimated VTA volumes (Fig. 3) suggested a reduction in median volume with the Anisotropic method. This trend was consistent with findings reported in [2]. Fig. 4 illustrates this qualitative similarity between results from literature and those obtained in the present study. This reduction in median volume warrants further investigation and should be paired with clinical outcomes to better understand DBS mechanisms where white

matter tracts are targeted. In contrast to anisotropy, the presence of scar tissue in the anisotropic model has a lower impact on the result.

A. Limitations

The anisotropic method required additional cost in terms of imaging data and computation with respect to similar VTA estimation methods. Furthermore, the scaling factor that mapped from diffusivity to conductivity was considered as a fixed value, independent of the fibre diameter. Thus, the assumption about fibre diameter was a critical choice. The scale factor from diffusivity to conductivity measures was set based on [23], which considers large size axons and this may have led to an overestimation of the conductivity values.

V. Conclusion

The main contribution of this work was the development of a patient-specific anisotropic VTA estimation method. It has been implemented in Lead-DBS and is publicly available. The method requires further testing with a larger cohort. This could be beneficial for DBS indications targeting white matter tracts.

Acknowledgment

The Neurosurgery and Neurology Departments at University Hospital of Bern provided data for testing. Johannes Vorwerk from University of Münster helped understand the SimBio/Fieldtrip LEAD-DBS functions.

References

[1] P. Krack, J. Volkmann, G. Tinkhauser, and G. Deuschl, "Deep Brain Stimulation in Movement Disorders: From Experimental Surgery to Evidence-Based Therapy," *Mov. Disord.*, vol. 34, no. 12, pp. 1795–1810, 2019.

[2] C. R. Butson, S. E. Cooper, J. M. Henderson, and C. C. McIntyre, "Patient-specific analysis of the volume of tissue activated during deep brain stimulation," *Neuroimage*, vol. 34, no. 2, pp. 661–670, 2007.

[3] B. Howell and C. C. McIntyre, "Analyzing the tradeoff between electrical complexity and accuracy in patient-specific computational models of deep brain stimulation," *J. Neural Eng.*, vol. 13, no. 3, pp. 1–17, 2016.

[4] A. Horn *et al.*, "Lead-DBS v2: Towards a comprehensive pipeline for deep brain stimulation imaging," *Neuroimage*, vol. 184, no. August 2018, pp. 293–316, 2019.

[5] T. A. K. Nguyen *et al.*, "Directional stimulation of subthalamic nucleus sweet spot predicts clinical efficacy: Proof of concept," *Brain Stimul.*, vol. 12, no. 5, pp. 1127–1134, Sep. 2019.

[6] J.-P. Lévy *et al.*, "Structure-function relationship of the posterior subthalamic area with directional deep brain stimulation for essential tremor," *NeuroImage Clin.*, vol. 28, p. 102486, 2020.

[7] J. N. Petry-Schmelzer *et al.*, "Network Fingerprint of Stimulation-Induced Speech Impairment in Essential Tremor," *Ann. Neurol.*, p. ana.25958, Nov. 2020.

[8] V. A. Coenen *et al.*, "Superolateral medial forebrain bundle deep brain stimulation in major depression: a gateway trial," *Neuropsychopharmacology*, vol. 44, no. 7, pp. 1224–1232, Jun. 2019.

[9] T. L. Chenevert, J. A. Brunberg, and J. G. Pipe, "Anisotropic diffusion in human white matter: demonstration with MR techniques in vivo.," *Radiology*, vol. 177, no. 2, pp. 401–405, Nov. 1990.

[10] J.-D. Tournier *et al.*, "MRtrix3: A fast, flexible and open software framework for medical image processing and visualisation," *Neuroimage*, vol. 202, p. 116137, Nov. 2019.

[11] M. Jenkinson, C. F. Beckmann, T. E. J. Behrens, M. W. Woolrich, and S. M. Smith, "FSL," *Neuroimage*, vol. 62, no. 2, pp. 782–790, Aug. 2012.

[12] J. Veraart, D. S. Novikov, D. Christiaens, B. Ades-aron, J. Sijbers, and E. Fieremans, "Denoising of diffusion MRI using random matrix theory," *Neuroimage*, vol. 142, no. 1, pp. 394–406, Nov. 2016.

[13] J. L. R. Andersson, S. Skare, and J. Ashburner, "How to correct susceptibility distortions in spin-echo echo-planar images: Application to diffusion tensor imaging," *Neuroimage*, vol. 20, no. 2, pp. 870–888, 2003.

[14] S. M. Smith *et al.*, "Advances in functional and structural MR image analysis and implementation as FSL," *Neuroimage*, vol. 23, no. SUPPL. 1, pp. 208–219, 2004.

[15] J. L. R. Andersson and S. N. Sotiropoulos, "An integrated approach to correction for off-resonance effects and subject movement in diffusion MR imaging," *Neuroimage*, vol. 125, pp. 1063–1078, 2016.

[16] K. G. Schilling *et al.*, "Synthesized b0 for diffusion distortion correction (Synb0-DisCo)," *Magn. Reson. Imaging*, vol. 64, no. December 2018, pp. 62–70, 2019.

[17] S. M. Smith, "Fast robust automated brain extraction," *Hum. Brain Mapp.*, vol. 17, no. 3, pp. 143–155, Nov. 2002.

[18] M. Jenkinson and S. Smith, "A global optimisation method for robust affine registration of brain images," *Med. Image Anal.*, vol. 5, no. 2, pp. 143–156, 2001.

[19] M. Jenkinson, P. Bannister, M. Brady, and S. Smith, "Improved Optimization for the Robust and Accurate Linear Registration and Motion Correction of Brain Images," *Neuroimage*, vol. 17, no. 2, pp. 825–841, 2002.

[20] Y. Zhang, M. Brady, and S. Smith, "Segmentation of brain MR images through a hidden Markov random field model and the expectation-maximization algorithm," *IEEE Trans. Med. Imaging*, vol. 20, no. 1, pp. 45–57, 2001.

[21] A. Barmpoutis and B. C. Vemuri, "A unified framework for estimating diffusion tensors of any order with symmetric positive-definite constraints," in *2010 IEEE International Symposium on Biomedical Imaging: From Nano to Macro*, 2010, pp. 1385–1388.

[22] A. P. Tran, S. Yan, and Q. Fang, "Improving model-based functional near-infrared spectroscopy analysis using mesh-based anatomical and light-transport models," *Neurophotonics*, vol. 7, no. 01, p. 1, Feb. 2020.

[23] D. S. Tuch, V. J. Wedeen, A. M. Dale, J. S. George, and J. W. Belliveau, "Conductivity tensor mapping of the human brain using diffusion tensor MRI," *Proc. Natl. Acad. Sci. U. S. A.*, vol. 98, no. 20, pp. 11697–11701, 2001.

[24] T. Susumu, Mori; J-Donald, Ed., "Mathematics of Diffusion Tensor Imaging," in *Introduction to Diffusion Tensor Imaging*, Elsevier, 2014, pp. 33–37.

[25] F. Rattay, "The basic mechanism for the electrical stimulation of the nervous system," *Neuroscience*, vol. 89, no. 2, pp. 335–346, Mar. 1999.

[26] M. Åström, E. Diczfalusy, H. Martens, and K. Wårdell, "Relationship between neural activation and electric field distribution during deep brain stimulation," *IEEE Trans. Biomed. Eng.*, vol. 62, no. 2, pp. 664–672, 2015.

[27] A. Horn *et al.*, "Connectivity Predicts deep brain stimulation outcome in Parkinson disease," *Ann. Neurol.*, vol. 82, no. 1, pp. 67–78, 2017.

[28] S. Ewert *et al.*, "Toward defining deep brain stimulation targets in MNI space: A subcortical atlas based on multimodal MRI, histology and structural connectivity," *Neuroimage*, vol. 170, no. May 2017, pp. 271–282, 2018.